Investigation of resonance-enhanced laser-induced breakdown spectroscopy for analysis of aluminium alloys

Goueguel, Christian; Laville, Stéphane; Vidal, François; Sabsabi, Mohamad; Chaker, Mohamed

Publisher's version / Version de l'éditeur:
https://doi.org/10.1039/b927013b
Journal of Analytical Atomic Spectrometry, 25, 5, pp. 635-644, 2010-05-01

JAAS

Journal of Analytical Atomic Spectrometry

www.rsc.org/jaas

Volume 25 | Number 5 | May 2010 | Pages 601–748

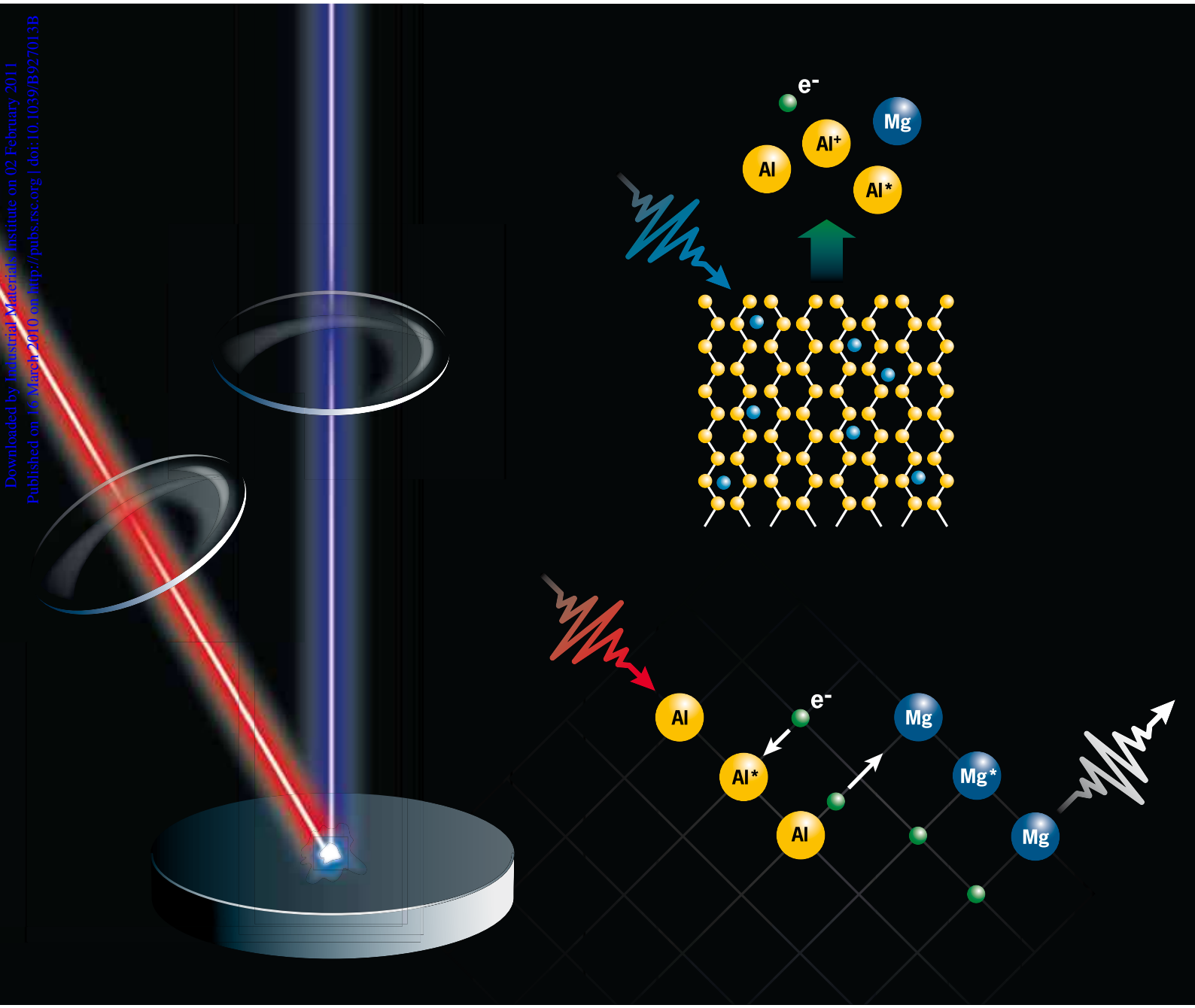

ISSN 0267-9477

RSC Publishing

Investigation of resonance-enhanced laser-induced breakdown spectroscopy for analysis of aluminium alloys

Christian Goueguel,[a] Stéphane Laville,[b] François Vidal,*[a] Mohamad Sabsabi[b] and Mohamed Chaker[a]

Received 22nd December 2009, Accepted 19th February 2010
First published as an Advance Article on the web 16th March 2010
DOI: 10.1039/b927013b

Resonance-enhanced laser-induced breakdown spectroscopy (RELIBS) was investigated with the aim to improve the limit of detection of trace elements in the context of elemental analysis of aluminium alloys. A Q-switched Nd:YAG laser pulse (7 ns, 1064 nm) was used for ablation of the samples and was followed, after a suitable delay, by an Optical Parametric Oscillator (OPO) laser pulse (7 ns), tuned at 396.15 nm, to resonantly excite the aluminium host atoms. In particular, the Mg I 285.21 nm and Si I 288.16 nm lines were observed in the acquisition spectral window. We investigated the influence of the main experimental parameters, namely, the excitation wavelength, the interpulse delay and the ablation and excitation fluences, on the signal-to-noise ratio for the Mg I 285.21 nm line. We found that, at low ablation fluences, typically less than a few J cm^{-2}, the Mg signal at 285.21 nm achieved using RELIBS was significantly enhanced when compared to LIBS using the same ablation fluence. At fluences higher than 8 J cm^{-2}, the effect of the excitation pulse became unnoticeable and similar results were observed for both approaches. The optimum conditions were achieved for an interpulse delay of about 30 ns, an ablation fluence of about 3.8 J cm^{-2} and an excitation fluence of about 1.1 J cm^{-2}. The corresponding absolute LoDs were 0.7 and 50 fg, for Mg and Si, respectively, using RELIBS. When using LIBS, they were 4 and 128 fg, instead. Finally, the applicability of RELIBS in the context of a minimally destructive elemental analysis is discussed.

A. Introduction

In laser-induced breakdown spectroscopy (LIBS), a powerful laser pulse is used to ablate and atomize material from the sample to analyze.[1–3] Both qualitative and/or quantitative information about the elemental composition of the sample can be rapidly obtained. The capabilities of LIBS to effectively carry out remote and real-time spectrochemical analysis on unprepared samples, for a wide variety of materials, make it a highly versatile analytical technique.[4,5] Nevertheless, it is generally acknowledged that the sensitivity of LIBS is relatively poor compared with other consolidated, but more cumbersome, atomic spectroscopy techniques.[5,6] Various options have been discussed in the literature to overcome this major drawback of LIBS. Techniques based on the use of two successive laser pulses are particularly interesting since they retain much of the advantageous features of single-pulse LIBS (*e.g.*, real time, remote, minimal sample preparation) while improving its analytical performances. In the two-pulse scheme, a first laser pulse is used to ablate the sample, and, after a certain delay, a second pulse is launched to excite the plasma.

The most common approach is probably the double-pulse (DP) LIBS in which the second laser pulse (generally a harmonic of the first pulse) is focused onto the plasma produced by the first pulse to increase the emission of the ablated material.[7–10] In the literature, emission enhancements up to 10-fold have been demonstrated for neutral species with respect to standard LIBS. This enhancement has been explained by a combination of an increase of material ablation and plasma volume, and reheating by the second pulse. (See ref. 8 for a review on the DP-LIBS approach.)

An important variant of the two-pulse scheme combines the advantages of LIBS with those of laser-induced fluorescence spectroscopy (LIF).[11–17] In the LIBS-LIF scheme, the second pulse, tuned to a specific transition wavelength of the analyte of interest, is used to enhance the fluorescence signal of the analyte and thus increase its signal-to-noise ratio (SNR). The optimal conditions are achieved for a cool and low-density atomic gaseous vapour of material, with enough atoms in the ground state to maximize the absorption of the second laser pulse. Analytical sensitivity has been shown to be improved up to three orders of magnitude in some cases with respect to LIBS in usual operating conditions (see ref. 14 and 15 for instance). The high performances of LIBS-LIF stem from the inherent high sensitivity and high selectivity that result from the excitation and detection schemes. However, in contrast with DP-LIBS, LIBS-LIF does not allow simultaneous multi-element analysis, which can be a severe limitation in some applications.

Recently, a new approach related to both LIBS-LIF and DP-LIBS, the resonance-enhanced LIBS (RELIBS) approach has been investigated by Cheung and co-workers.[18–23] In RELIBS, the second pulse is tuned to the wavelength of a resonant atomic transition of the matrix atoms of the plasma instead of a particular analyte, as in LIBS-LIF. The energy absorbed in a selected atomic state is then distributed over all other elements through

[a]*INRS Énergie, Matériaux et Télécommunications, 1650 Lionel-Boulet Blvd, Varennes, Québec, Canada J3X 1S2. E-mail: vidal@emt.inrs.ca; Fax: (+1)450 929 8102; Tel: (+1)450 929 8118*
[b]*National Research Council of Canada, Industrial Materials Institute, 75 de Mortagne Blvd., Boucherville, Québec, Canada J4B 6Y4*

particle–particle collisions, as in DP-LIBS. To the best of our knowledge, only a few papers have been devoted to RELIBS. Chan and Cheung[22] explored the ability of RELIBS for the analysis of small amount of sodium in potassium iodate samples. A hot plasma plume was produced with an intense 532 nm laser pulse followed by a non-ablative dye laser pulse tuned at 404.4 nm for resonant excitation of potassium. They found out that the 589 nm emission of sodium was significantly enhanced and they estimated the absolute limit of detection to be 5-fold lower than that obtained by LIBS. Similarly, Lui and Cheung[20] observed noticeable enhancements in emission intensity of several trace components (Mg, Cu, Si and Na) in aluminium alloys when the second laser pulse was tuned to the Al I 396.15 nm resonant transition. They found out that the use of ablation fluences close to the ablation threshold was necessary to optimize RELIBS as the enhancement effect disappeared for much higher values. These investigations have pointed out the potential of RELIBS for improving sensitivity in the context of a minimally destructive analysis without any loss of LIBS advantages.

It is worth noting that selective excitation can also be performed using a single laser pulse *via* the resonant laser ablation (RLA) scheme.[24–26] In RLA the ablation wavelength is tuned either on a resonant transition of the analyte,[24] as in LIBS-LIF, or of the matrix atoms,[25,26] as in RELIBS. Despite its greater simplicity, in RLA the excitation delay time cannot be controlled as in LIBS-LIF and RELIBS as it is completely determined by the pulse duration of the ablation/excitation pulse. To our knowledge, LIBS based on a single resonant ablation pulse for analytical purposes has not been investigated yet, and this scheme is presently under evaluation in our group.

According to ref. 18–23, RELIBS appears to be a great candidate for applications where damage inflicted to the sample must be minimized. In this context, a better understanding of the mechanisms involved in RELIBS is required to improve the analytical features of this technique. Up to now, very little work was done on RELIBS, in particular, to clarify the plasma conditions to be achieved to optimize the SNR for the analyte signals.

In this paper, we present a comprehensive parametric investigation of the signal-to-noise ratio (SNR) for the Mg I 285.21 nm line using the RELIBS scheme in aluminium alloys. For that purpose, we discuss the influence of the main experimental parameters, namely (1) the excitation wavelength, (2) the temporal delay between the ablation and excitation pulses (interpulse delay), (3) the excitation fluence and (4) the ablation fluence. The analytical figures of merit achieved using RELIBS will also be compared to those of LIBS for simultaneous detection of Mg and Si, using the Mg I 285.21 nm and Si I 288.16 nm lines, respectively.

B. Experimental setup

A detailed schematic of the experimental arrangement used in this work is presented in Fig. 1. The ablation was performed using a Q-switched Nd:YAG laser (Surelite I-10, Continuum). The wavelength was 1064 nm while the pulse width at full-width-half-maximum (FWHM) was 7 ns. In order to ensure a good spatial profile, the beam spot was reshaped using an iris diaphragm, prior to being focused onto the sample using a plano-convex spherical BK7 lens (25.4-mm diameter and 150-mm focal length) at normal incidence to the sample. The experiments were performed in air at atmospheric pressure and the repetition rate was 5 Hz. An extractor fan was also positioned next to the plasma to limit the interaction between both lasers and aerosols and improve the shot-to-shot reproducibility. The ablation laser spot on the surface of the sample was circular and its diameter was estimated to be about 100 μm. For this estimation, three-dimensional (3-D) crater images were acquired for several ablation energies using an in-house built profilometer based on optical coherence tomography (OCT).[27] (These images were also used to estimate the ablated volume—see Sec. C.6) Then, the procedure described in ref. 28 and 29 was followed, assuming the beam to be spatially Gaussian. (The radius of the laser spot corresponds to the slope of the radius of the ablation crater plotted as a function of the logarithm of the laser energy.) In these experiments, the ablation fluence (F_{ABL}) was varied from about 0.4 to 30 J cm^{-2}.

The excitation laser pulse was delivered by an Optical Parametric Oscillator (OPO) laser (Panther OPO PL8000, Continuum). The pulse duration was 7 ns and the repetition rate

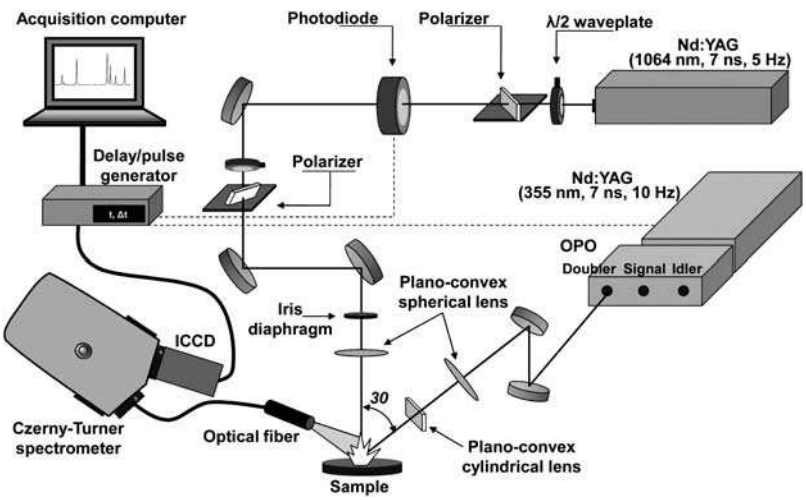

Fig. 1 Schematic of the experimental set-up.

was 10 Hz. The OPO laser was pumped by a 355 nm frequency tripled Q-switched Nd:YAG laser with energy of about 250 mJ per pulse. At the various outputs of the OPO (doubled signal or idler, signal and idler—see Fig. 1), the wavelength of the laser pulse can be tuned from 215 nm to 2.7 μm and the corresponding output energy per pulse ranges from 9 to 22 mJ in the infrared, 1 to 70 mJ in the visible and from 0.01 to 15 mJ in the ultraviolet. The wavelength can be adjusted through a computer interface enabling scan rates of 0.2 nm s^{-1} with an accuracy of 0.01 nm. The excitation beam was focused into the plasma plume using a spherical plano-convex fused silica lens (100-mm focal length and 25.4-mm diameter). The angle between the ablation and the excitation laser beams was fixed to about 30°. In order to achieve a more reliable coupling between the OPO beam and the plasma, the OPO spot was reshaped by using a cylindrical plano-convex fused silica lens (129-mm focal length, 40 × 25.4-mm dimensions), positioned between the focusing lens and the sample. The resulting average spot on the surface of the sample was an ellipse whose dimensions of 136 μm × 178 μm were comparable with the ablation spot dimensions. (The excitation spot dimensions were measured using the same procedure as the ablation laser spot.) The excitation fluence (F_{EXC}) on the sample surface was varied from about 0.02 to 4.3 J cm^{-2}. The excitation energy was adjusted using a set of neutral density filters.

Synchronization of the two laser pulses was achieved using an 8-channel programmable delay generator (model 565, Berkeley Nucleonics Corporation) that was triggered by a high speed photodiode detector (model 301-020R, Scientech Inc.). Energy of both lasers was measured with a low energy pyroelectric head detector (PE10-SH-v2, Ophir Optronics Ltd.) connected to a laser power/energy display (Nova II, Ophir Optronics Ltd). The interpulse delay was varied from 0 ns (*i.e.*, simultaneous pulses) to 100 ns.

The light collection was performed using an optical fiber (600 μm core diameter) positioned a few millimetres away from the plasma plume and connected to the entrance slit of a Czerny–Turner spectrometer (VM504, Acton Research Corp.). Its focal length was 0.39 m and its *f*-number was 5.4. The spectrometer was equipped with a grating of 1200 lines/mm blazed at 150 nm. The corresponding linear dispersion was about 2.1 nm mm^{-1}. The exit slit was coupled to an Intensified CCD camera (model DH720-25*H*-05, Andor iStar) containing 1024 × 256 pixels of 26 μm^2 dimensions. The photocathode of the intensifier was thermo-electrically cooled down to −6 °C to reduce the thermal noise. The width of the entrance slit was 300 μm. The spectral width of the intensified acquisition window was about 56 nm while the spectral resolution was about 0.16 nm. The fluorescence signal was acquired starting 10 ns after the beginning of the excitation pulse so that the acquisition delay was equal to the interpulse delay + 10 ns, while the gate width was fixed to 3 μs. Finally, a fused silica short-pass filter/UV 350-nm (XUS0350, Asahi Spectra Inc., USA) was installed at the entrance slit of the spectrometer to attenuate the scattered laser light due to the excitation pulse during the acquisition temporal gate.

The parametric study was performed using a certified aluminium alloy sample provided by Rio Tinto Alcan Inc. (standard 356.2 AH) containing 0.42% of magnesium. This sample was selected to provide a high SNR for the Mg I 285.21 nm line in all our experimental conditions while maintaining self-absorption of this line to a reasonable level (see Sec. C.6 for a more detailed discussion). To plot the calibration curves for Mg and Si, a set of 10 aluminium alloy samples were used, with concentrations of Mg ranging from 0.0041% to 2.51%, and those of Si from 0.087% to 9.63%.

Prior to any acquisition, 500 cleaning shots were performed to remove surface contaminants. Then, 500 acquisition shots were performed at each of three sites on the sample surface distant of a few millimetres to take into account any lack of homogeneity. A double axis motorized stage (model UTM100C-C1HL, Newport) controlled by a programmable motion controller/driver (model ESP300, Newport) was used to move the sample from site to site.

C. Results and discussion

The laser-induced atomic transitions used in this work are given in the partial Grotrian diagram shown in Fig. 2. The OPO laser, tuned at 396.15 nm, excites the Al neutrals from the state $^2P^o_{3/2}$ to the upper state $^2S_{1/2}$. Then, the higher $^2P^o_1$ level of Mg is excited either by free electrons having undergone superelastic collisions with the excited Al neutrals (*i.e.*, collisions in which the incident electrons gain the excitation energy of the excited Al atoms) or by direct collisions of the Mg atoms with the excited Al atoms. The 1.2 eV energy gap between the Mg $^2P^o_1$ state and the Al $^2S_{1/2}$ level can be filled for example by particles having undergone multiple superelastic collisions. The free electrons mainly come from the plasma produced by the ablation pulse or by the excitation pulse through photoionization or collisional ionization when the laser intensity is high enough. Then, Mg atoms decay to their ground state ($^1S_0$) by emitting a fluorescence signal at 285.21 nm. The 396.15 nm line was selected mainly because of its high spontaneous emission probability equal to 9.80 × 10^7 s^{-1}.[30]

In the following, we report on the influence of the main experimental parameters, namely, (1) the excitation wavelength, (2) the interpulse delay, (3) the excitation fluence and, (4) the ablation fluence, on the signal-to-noise ratio (SNR) for the Mg I 285.21 nm line in aluminium alloys using the RELIBS scheme. This study allowed determining the optimum plasma conditions

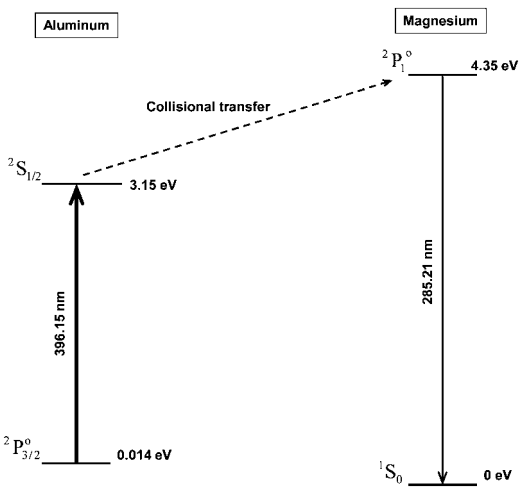

Fig. 2 Partial Grotrian diagram for excitation of magnesium from selective excitation of aluminium atoms.

for efficient spectrochemical analysis and comparing the figures of merit of RELIBS with those of LIBS for analytical purposes.

The optimal conditions for RELIBS that resulted from this study are: an excitation fluence of 1.1 J cm^{-2}, an ablation fluence of 3.8 J cm^{-2} and an interpulse delay of 30 ns. The optimal wavelength was obtained at peak of the strong Al I 396.15 nm line. In this section these parameters will be varied around these values and the results will be discussed in light of the underlying physical mechanisms at play in RELIBS.

C.1 Wavelength dependence

To demonstrate the spectral selectivity of the RELIBS scheme, we show in Fig. 3 the SNR for the Mg I 285.21 nm fluorescence signal as a function of the excitation wavelength. The noise measurements were carried out by tuning the excitation wavelength to 400 nm. We checked out that, over the spectral range presented here, the excitation laser spot was not notably displaced by the optical parametric conversion process by watching optical images of the craters produced by numerous laser shots.

As a feature of a resonance phenomenon, a strong increase of the SNR of the Mg I 285.21 nm line is observed in Fig. 3 when the excitation wavelength matches the intense aluminium lines at 394.42 nm and 396.15 nm. This corresponds to the $^2P^o_{1/2} \rightarrow {}^2S_{1/2}$ and $^2P^o_{3/2} \rightarrow {}^2S_{1/2}$ transitions involved in the fine structure doublet of the Al atom. Such spectral selectivity cannot be achieved in the DP-LIBS approach for which the wavelength of the 2nd pulse is generally a harmonic (off resonance) of the available laser system. Therefore, Fig. 3 clearly demonstrates that a RELIBS effect, and not a DP-LIBS effect, takes place in our experiments.

The ratio between the Mg I 285.21 nm fluorescence signals for the 394.40 nm and the 396.15 nm excitation wavelengths, is nearly equal to 2, which corresponds to the ratio between the radiative transition probabilities (4.93×10^7 s^{-1} and 9.80×10^7 s^{-1}, respectively).[30] This result suggests that the collisional de-excitation rates are much lower than the radiative de-excitation rates or that the collisional rates are in the same proportion with respect to the corresponding radiative rates. The deconvolution of these two overlapping profiles, assumed to be Lorentzian as a first approximation, was carried out to estimate their width, which was found to be about 1 nm at FWHM for both profiles. This relatively broad bandwidth is likely due to combination of Stark broadening and saturation broadening[31] (in the context of LIF) of both Al and Mg states.

Consequently, in order to maximize the SNR for the Mg I 285.21 nm line, the excitation wavelength must be tuned to the strong Al I 396.15 nm transition. In the following, the Mg fluorescence signals obtained when the excitation is on resonance (396.15 nm) and off resonance (400 nm) will be compared.

C.2 Interpulse delay

In Fig. 4, we present the SNR for the Mg I 285.21 nm line, achieved by RELIBS, as a function of the interpulse delay for three ablation fluences.

One can see in Fig. 4 that the SNR for the Mg I 285.21 nm line is maximized for an interpulse delay of about 30 ns, for ablation fluences of 5.1 and 8.5 J cm^{-2}. For the lowest fluence (2.6 J cm^{-2}), the maximum is not as well defined but seems to be between 0 and 30 ns. Consequently, the optimum interpulse delay is in the range of 20–30 ns. This result is in agreement with the value of 30 ns also reported in ref. 20 in aluminium samples and pellets of potassium idoate[18,19,21,22] under comparable experimental conditions.

A similar behaviour has already been observed using the LIBS-LIF scheme (see ref. 14 for instance). However, the optimum interpulse delay was of the order of several μs for ablation fluences of a few J cm^{-2}. This large discrepancy is mainly due to the differences in the excitation mechanisms involved in LIBS-LIF and RELIBS. Indeed, in LIBS-LIF the fluorescence signal is basically optimized when the population, generally in the ground

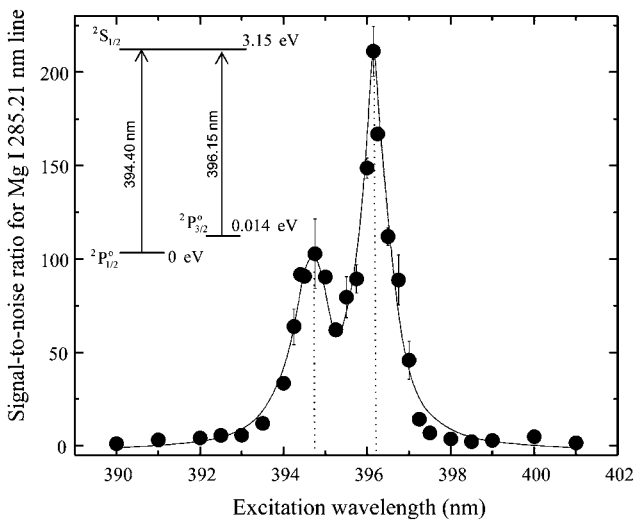

Fig. 3 SNR for the Mg I 285.21 nm line as a function of the excitation wavelength. The ablation fluence was 3.8 J cm^{-2} and the excitation fluence was 1.1 J cm^{-2}. The interpulse delay was 30 ns. The inset shows a partial Grotrian diagram for aluminium.

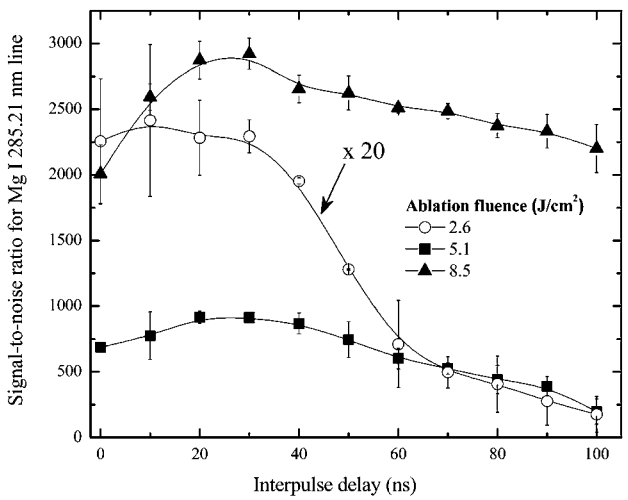

Fig. 4 SNR for the Mg I 285.21 nm line as a function of the interpulse delay for an excitation fluence of 1.1 J cm^{-2} and ablation fluences of 2.6, 5.1 and 8.5 J cm^{-2}. The excitation wavelength was tuned to 396.15 nm. (Note that curve at 2.6 J cm^{-2} was magnified by 20 to ease the visualization).

state, of the analyte under study, is maximized. Consequently, a low plasma temperature must be reached, which generally occurs after a relatively long delay. Instead, in RELIBS, a compromise must be established between the population of the matrix element in the ground level and the electron density since the energy transfer from the major element to the analytes, which follows resonant absorption, likely takes place mainly through collisions involving the electrons. After the excitation pulse, the de-excitation rate of the excited Al atoms can be expressed as:

$$\frac{dn_{exc}}{dt} \approx -kn_e n_{exc} - An_{exc} \quad (1)$$

where n_{exc} is the density of excited Al atoms, k is the parameter characterizing collisional de-excitation, n_e is the electron density, and A is the spontaneous radiation decay. One can see that if $kn_e \ll A$, most of the excited states would de-excite radiatively and the excitation energy of the Al atoms would not be transferred to the analytes. (Even with re-absorption the emitted radiation eventually escapes the medium.) Consequently, a relatively high electron density, which is generally associated with a high plasma temperature, is required, justifying a lower interpulse delay when compared to LIBS-LIF.

Fig. 4 also shows that, for a given interpulse delay, the SNR for the Mg I 285.21 nm line increases with the ablation fluence. This result can be explained by the fact that the amount of ablated matter increases with the ablation fluence, so that more Mg atoms can be excited and participate to the fluorescence signal.

C.3 Excitation laser fluence

Fig. 5 shows the SNR for the Mg I 285.21 nm line, as a function of the excitation fluence. (Note that the SNR was increased by 1 to enable the representation on the log-log scale.) The results are shown for RELIBS using two excitation wavelengths: one tuned at the Al I 396.15 nm line (on resonance) and the other one at 400 nm (slightly off resonance). To evaluate the influence of the excitation pulse alone, we also show the Mg signal obtained with the excitation pulse without the ablation pulse for both wavelengths.

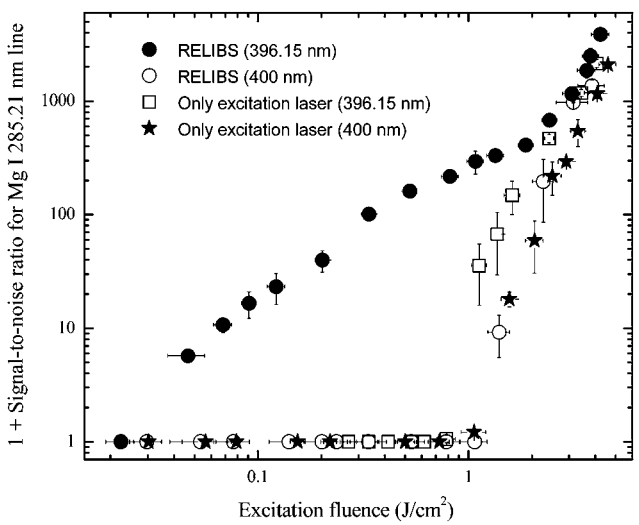

Fig. 5 SNR + 1 for the Mg I 285.21 nm fluorescence signal as a function of the excitation fluence. Using RELIBS, the excitation wavelength was tuned on resonance (at 396.15 nm) and off resonance (at 400 nm). The ablation fluence was 3.8 J cm^{-2}. The interpulse delay was 30 ns. The Mg signals obtained with only the excitation pulse for both wavelengths are also shown.

One can see in Fig. 5 that when the excitation pulse was tuned off resonance (at 400 nm), no fluorescence signal was measured below 1.1 J cm^{-2} with or without the ablation pulse. In presence of the ablation pulse, the 400 nm photons clearly go through the plasma without being absorbed by the aluminium atoms. For higher excitation fluences, the SNR strongly increases since the excitation pulse starts to ablate the sample.

When the excitation pulse is on resonance and interacts with the plasma produced by the ablation pulse, the SNR is not zero below 1.1 J cm^{-2}, which means that the excitation pulse interacts resonantly with the Al I atoms of the plasma. A clear transition can be seen near a value of 1.9 J cm^{-2} as the slope of the SNR is about 0.65 on the log-log scale just below 1.9 J cm^{-2}, while it reaches about 5 above 3.2 J cm^{-2}. This slope is almost the same as that of the SNR when the pulse is off resonance (as well as the SNR without the ablation pulse). This suggests that the increase of the SNR in the case of on resonance RELIBS is due to an increase of the ablation by the excitation pulse. Therefore, the excitation beam is not completely absorbed in the plasma and a significant fraction is able to reach the sample surface. This could well occur when all the neutral Al atoms are excited so that the plasma can no longer absorb resonantly the excitation pulse. Indeed, the near saturation of the SNR observed between 1 and 2 J cm^{-2} indicates that most of the available atoms have been excited. In addition, a transition is observed only at 1.9 J cm^{-2} instead of 1.1 J cm^{-2} since the second ablation contribution starts to be comparable to the RELIBS contribution only near 1.9 J cm^{-2}, as can be seen on the case without the ablation pulse.

In the absence of the ablation pulse, the SNR achieved when the excitation pulse is tuned on resonance starts to increase at a lower excitation fluence (about 0.8 J cm^{-2}) than when off resonance (resp., about 1.1 J cm^{-2}). This value of 1.1 J cm^{-2} is comparable to the value of 1.3 J cm^{-2} for the ablation threshold reported in ref. 32 for a wavelength of 532 nm and a similar pulse duration. Still in the absence of the ablation pulse, it is interesting to note that, when the excitation fluence remains weak (typically between 1.1 and 2.0 J cm^{-2}), the SNR is notably higher when the excitation is on resonance. For instance, for an excitation fluence of 1.3 J cm^{-2}, the SNR varies from 10 (off resonance) to 70 (on resonance). This effect originates from a RLA effect, as discussed in the introduction.

In the following, a value of 1.1 J cm^{-2} for the excitation fluence was considered since it produced the highest SNR for the Mg I 285.21 nm line and was somewhat below the ablation threshold of aluminium to prevent any extra ablation from the sample.

C.4 Ablation laser fluence

Fig. 6 shows the SNR for the Mg I 285.21 nm line, as a function of the ablation fluence. The measurements were conducted for the 396.15 nm (on resonance) and 400 nm (off resonance) excitation wavelengths. The excitation fluence was 1.1 J cm^{-2} for which the ablation induced by the excitation pulse remained

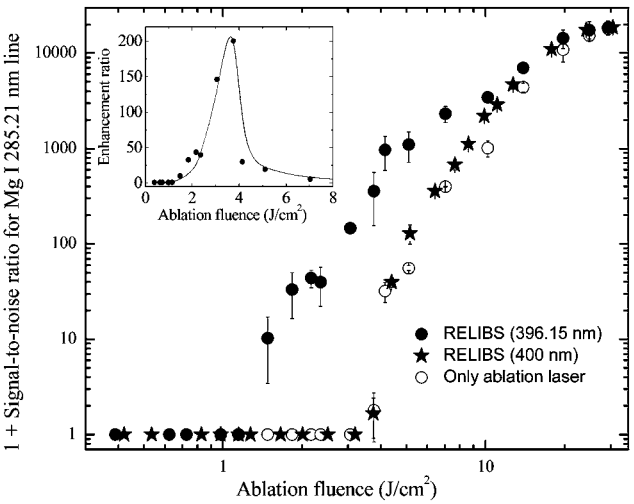

Fig. 6 SNR + 1 for the Mg I 285.21 nm line as a function of the ablation fluence. The wavelength of the excitation pulse was set either on resonance (at 396.15 nm) or off resonance (at 400 nm). The excitation fluence was 1.1 J cm^{-2} and the interpulse delay was 30 ns. The case with only the ablation pulse is also shown. The inset shows the enhancement ratio between RELIBS (at 396.15 nm) and the case with only the ablation pulse.

insignificant (see Sec. C.3). The results obtained with only the ablation pulse are also shown for comparison.

One first observes that the SNR in LIBS (only ablation pulse) and RELIBS with an off-resonance excitation pulse are almost identical. This indicates that the effect of the excitation pulse on the SNR is negligible when tuned off resonance. In both cases, the SNR exhibits a clear threshold near about 3.8 J cm^{-2}, which is approximately three times higher than the ablation threshold of 1.01 J cm^{-2} reported in the literature for the same wavelength and pulse duration.[32] This discrepancy comes from the fact that a higher fluence is required to generate plasma that emits a detectable amount of radiation. The SNR increases rapidly with the ablation fluence, as a consequence of the rise in the amount of ablated matter and of the plasma temperature, and then saturates near 20 J cm^{-2}.

When the excitation pulse is tuned on resonance, one observes a high SNR, even at fluences lower than 3.8 J cm^{-2}. This clearly indicates that matter is actually ablated by the ablation pulse for fluences lower than 3.8 J cm^{-2} but that the ablated matter is too tenuous and cold to provide a detectable Mg I 285.21 nm fluorescence signal. The on-resonance excitation pulse is thus able to excite and heat this ablated matter (and possibly to enhance ablation) to produce a detectable fluorescence signal. The SNR with the on-resonance excitation pulse increases with the ablation fluence and starts saturating near 6–7 J cm^{-2}. It is likely that for those fluences the plasma is so hot that too few atoms are in the aluminium $^2P^o_{3/2}$ state to be excited efficiently by the on-resonance pulse. However, past the ablation fluence of 10 J cm^{-2}, the SNR starts to increase faster and to follow closely the SNR obtained without the excitation pulse or with an off resonance excitation pulse. In this regime, the effect of the on resonance pulse is negligible and the SNR is essentially due to the ablation pulse, as in LIBS.

The inset in Fig. 6 represents the enhancement ratio, which is defined as the ratio between the SNR + 1 achieved with on resonance RELIBS and the SNR + 1 with LIBS (*i.e.*, without the excitation pulse), as a function of the ablation fluence. One can see that the optimum value of the enhancement ratio is about 200 and occurs for an ablation fluence of about 3.8 J cm^{-2}. It should be noted that this value depends somewhat on the definition used for the enhancement ratio that could have also been defined by the ratio of both SNRs. In that case, the optimum ablation fluence would have been about 3.2 J cm^{-2}, corresponding to the highest value of fluence for which the SNR with LIBS is zero.

C.5 Damage to the samples

In the previous section, we showed that the maximum enhancement ratio of RELIBS with respect to LIBS is obtained for ablation fluence close to the threshold for the Mg fluorescence signal (*i.e.*, 3.8 J cm^{-2} in our case). As a consequence, RELIBS appears to be particularly relevant for minimally destructive elemental analysis.

In this context, it is essential to relate the RELIBS signal with the damage inflicted to the sample. In order to verify the correlation between the ablated mass and the RELIBS signal enhancement in our experiments, a confocal microscope (Nikon Eclipse ME600) with a 10×/0.30 objective and equipped with a 3-CCD color video camera (DXC-950P, Sony Corp.) was used. Using this microscope, the ablation craters resulting from 1000 laser pulses on the polished surface of an aluminium sample were compared.

Fig. 7 shows the optical images of the ablation craters (left) for ablation fluences of (a) 1.5, (b) 3.8 and (c) 13.9 J cm^{-2}. For each ablation fluence, we also show three corresponding spectra (right) in the 281–291 nm range (in which the Al II 281.62 nm, Mg I 285.21 nm, and Si I 288.16 nm lines can be seen). These three spectra were obtained using (1) only the on-resonance excitation pulse, (2) only the ablation pulse and, (3) RELIBS with an on-resonance excitation.

As can be seen from the optical images of craters of Fig. 7 (left) the ablation craters are circular and the diameters are of the order of 100 μm, as mentioned in Sec. B. From the spectra in Fig. 7 (right) one can see that the excitation pulse alone has a negligible effect on the sample since no emission was observed. (This was confirmed by optical images of craters where surface damage was not significant.) However, when using an ablation fluence of 1.5 J cm^{-2}, both the Mg I 285.21 nm and Si I 288.16 nm lines were observable by RELIBS even if no visible damage was induced on the surface of the aluminium sample. At 3.8 J cm^{-2}, surface melting became apparent and signals for Mg I 285.21 nm, Si I 288.16 nm and Al II 281.62 nm lines became drastically more intense for on-resonance excitation. In contrast, these lines recorded with only the ablation pulse remained undistinguishable from the background noise. At 13.9 J cm^{-2}, surface damage became relatively extensive. As a result, the contrast between RELIBS and the case with only the ablation pulse (LIBS) decreased significantly. Fig. 7 confirms the conclusion drawn in section C.4 that the ablation fluence is a very critical parameter to the RELIBS phenomenon, as emission signal enhancements disappear for high ablation fluences.

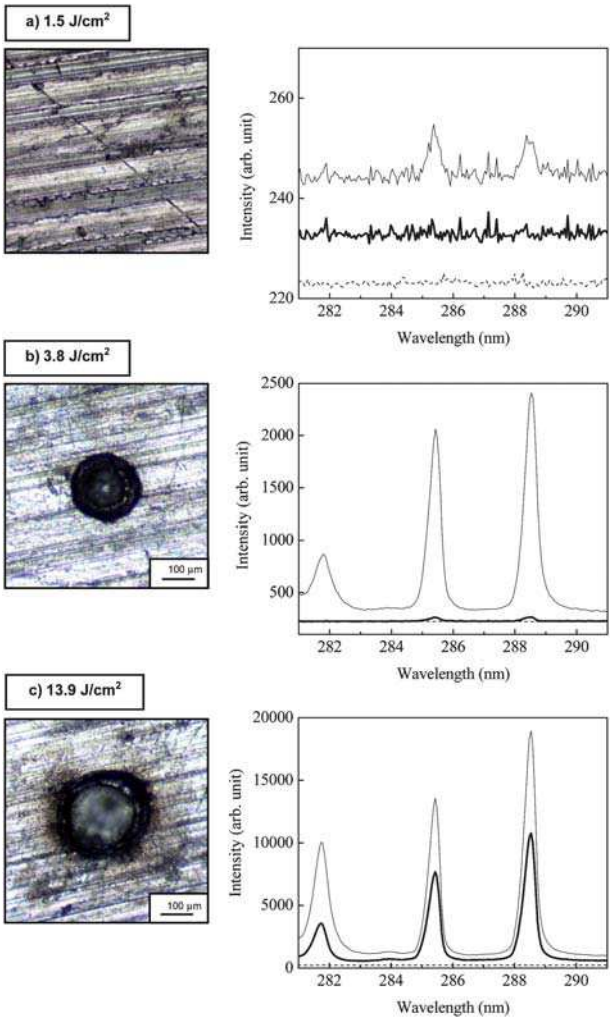

Fig. 7 (Left) Optical images of craters produced on an aluminium sample using 1000 laser shots at fluences of (a) 1.5, (b) 3.8 and (c) 13.9 J cm^{-2}, at a wavelength of 1064 nm. (Right) Corresponding spectra in the 281–291 nm range acquired by using only the on-resonance excitation pulse (**---**), only the ablation pulse (**—**) and, RELIBS with an on-resonance excitation (—). The excitation fluence was 1.1 J cm^{-2}. Each spectrum was an accumulation over 500 acquisition shots. Note that for visual clarity, a vertical offset was applied only on spectra for case (a).

An interesting feature of Fig. 7 is that, despite the signal intensity enhancement in RELIBS, the background intensity remains the same as when using only the ablation pulse. This indicates that the excitation pulse has a very small effect on the overall plasma temperature and electron density.

C.6 Analytical figures of merit

The parametric study presented in the previous sections allowed us to identify the experimental parameters for maximizing the SNR for the Mg I 285.21 nm line achieved by RELIBS. In order to evaluate the potential of RELIBS for multi-element analysis, we investigate in this section the simultaneous detection of magnesium and silicon in aluminium samples. In doing so we implicitly assume that the optimal parameters identified in the previous sections for the Mg line also hold approximately for the chosen Si line.

Fig. 8 shows the calibration curves for the Mg I 285.21 nm (a) and Si I 288.16 nm (b) lines, where intensities were normalized by the Al I 266.04 nm line. However, instead of using a shot-to-shot normalization, we preferred using the ratio of the intensities averaged over 500 shots due to single-shot weak signals for the Mg and Si lines.

In Fig. 8a, the calibration curve for the Mg I 285.21 nm line exhibits a linear behaviour for low concentrations (up to about 0.1%), and departs from linearity for higher concentrations due to self-absorption (see inset). Consequently, for the sample containing 0.42% of Mg that was used in the parametric study (see Sec. C.1 to C.5), self-absorption was not negligible. This observation should have no consequence on the optimum parameters previously determined. Indeed, to achieve an efficient RELIBS scheme, the excitation fluence should remain relatively weak (*cf.* Sec. C.3) so that self-absorption is mainly affected by the ablation fluence. Consequently, when comparing RELIBS (at 396.15 nm) and LIBS, self-absorption is basically similar. Then, the calibration curve for the Si I 288.16 nm line (Fig. 8b) exhibits a linear trend ($R^2 \approx 0.99$) over the whole range of concentrations taking into account the experimental uncertainties.

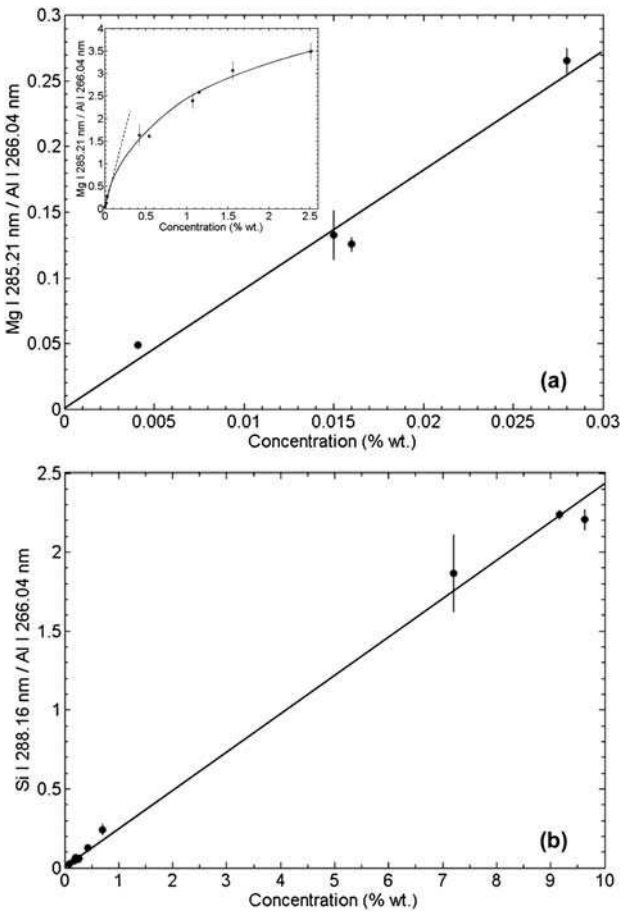

Fig. 8 Calibration curves for the Mg I 285.21 nm (a) and Si I 286.16 nm (b) lines achieved by RELIBS. Each mean intensity was normalized by those of the Al I 266.04 nm line. The ablation fluence was 3.8 J cm^{-2} and the excitation fluence was 1.1 J cm^{-2}. The interpulse delay was 30 ns.

Table 1 Limit of detection for the Mg I 285.21 nm and Si I 288.16 nm lines using LIBS and RELIBS for ablation fluences of 25.5 and 3.8 J cm^{-2}. For RELIBS, results are shown for excitation fluences of 1.1 and 2.8 J cm^{-2}. The absolute LoDs are also given in parentheses

		Ablation fluence/J cm^{-2}	
		3.8	25.5
		LoD (abs. LoD)	LoD (abs. LoD)
LIBS	Mg	>0.42% (>147 fg)	6 ppm (4 fg)
	Si	>7.2% (>2500 fg)	186 ppm (128 fg)
RELIBS (F_{EXC} = 1.1 J cm^{-2})	Mg	21 ppm (0.7 fg)	Not determined
	Si	1438 ppm (50 fg)	
RELIBS (F_{EXC} = 2.8 J cm^{-2})	Mg	Not determined	3 ppm (2 fg)
	Si		45 ppm (31 fg)

In order to fully evaluate the potential of RELIBS for analytical purposes, we present, in Table 1, the LoDs for the Mg I 285.21 nm and Si I 288.16 nm lines achieved using RELIBS and LIBS for two ablation fluences: 3.8 and 25.5 J cm^{-2}. The value of 3.8 J cm^{-2} corresponds to the optimum ablation fluence found for RELIBS in section C.4 while the value of 25.5 J cm^{-2} was chosen because of its representativeness for LIBS applications. When using RELIBS, the excitation pulse was tuned at 396.15 nm and the excitation fluences were 1.1 and 2.8 J cm^{-2}. The values of the LoDs were calculated on the basis of the IUPAC 3σ-convention, where σ is the standard deviation of the background noise. To do so, the SNRs corresponding to the sample containing 0.028% of Mg and to the one containing 0.7% of Si were considered. For both samples, the fluorescence signals appeared sufficiently intense to be reliable while maintaining a concentration of each analyte into the linear part of the calibration curve—See Fig. 8. The absolute LoDs are also indicated in parentheses and will be discussed thereafter.

Table 1 shows that for high ablation fluence (F_{ABL} = 25.5 J cm^{-2}), the LoDs obtained with both techniques (F_{EXC} = 2.8 J cm^{-2}) are basically of the same order. Indeed, values of about 6 and 3 ppm were achieved for Mg, while they were 186 and 45 ppm for Si, with LIBS and RELIBS, respectively. However, at low ablation fluence (3.8 J cm^{-2}), the LoD is improved by several orders of magnitude using RELIBS (F_{EXC} = 1.1 J cm^{-2}), when compared to LIBS. Indeed, the LoDs obtained with RELIBS were 21 and 1438 ppm, for Mg and Si, respectively. When using LIBS at 3.8 J cm^{-2}, the exact values of the LoDs were not estimated here due to the lack of suitable samples but were well above 0.42% and 7.2%, respectively.

These results confirm once again that the RELIBS scheme is much more efficient, than LIBS, at low ablation fluences. However, the LoDs achieved here by LIBS (F_{ABL} = 25.5 J cm^{-2}) were better when compared with RELIBS in the optimum conditions (F_{ABL} = 3.8 J cm^{-2} and F_{EXC} = 1.1 J cm^{-2}), a result which might seem quite surprising and misleading. However, as we will show in the following, in order to clearly extract the potential of RELIBS and perform a fair comparison with LIBS, the absolute LoDs achievable with both techniques should be compared instead of the relative LoD. The absolute LoD represents the minimum amount of ablated matter that can be measured with our setup. It is defined by the product of the amount of ablated matter per pulse with the limit of detection. Indeed, it appears that there is a large difference in the amount of ablated matter with both techniques (F_{ABL} = 25.5 J cm^{-2} *versus* 3.8 J cm^{-2}), justifying the comparison of absolute LoDs instead of relative LoDs.

A similar conclusion about comparison of RELIBS and LIBS was drawn in ref. 20 for the detection of Na in aluminium alloys. The LoD obtained for Na based on the Na I 589.9 nm line was 0.15 ppm using RELIBS with an ablation fluence of 3.2 J cm^{-2} (Nd:YAG at 532 nm) and an excitation fluence of 35.4 mJ cm^{-2}. (The spot diameters were 100 μm and 600 μm, respectively.)

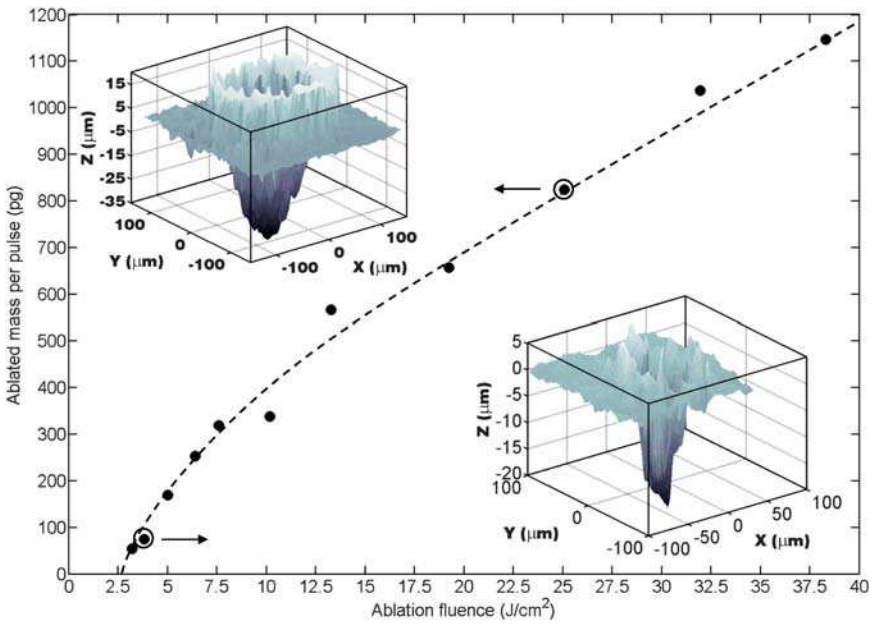

Fig. 9 Measured ablated mass removed per laser shot as a function of the ablation fluence. (The dashed line represents a guide for the eye.) These values were determined by averaging over 1000 laser shots. 3-D images of the crater are also shown for ablation fluences of 3.8 J cm^{-2} and 25.5 J cm^{-2}.

Using LIBS with an ablation fluence of 16 J cm^{-2}, a value of 0.075 ppm was achieved. The measured ablation rate was 2 ng/pulse at 3.2 J cm^{-2} and 8 ng/pulse at 16 J cm^{-2}, so that the absolute LoDs were 0.3 fg with RELIBS and 0.6 fg with LIBS.

It should be pointed out that the LoD for Si achieved using RELIBS is much higher than the LoD for Mg. This simply results from the fact that the spontaneous emission coefficient for Mg line is much higher than Si line.

Fig. 9 shows the measured ablated mass removed from the sample per laser shot as a function of the ablation fluence. The ablation volume was obtained by averaging over 1000 laser shots and using 3-D images of the craters measured using OCT technique (see Sec. B).

From Fig. 9, one can clearly see that the ablated mass per pulse increases non-linearly with the ablation fluence and rise at about 2.6 J cm^{-2}, corresponding to the ablation threshold. This value is similar to the value of 3.8 J cm^{-2} for the emission of the Mg line, obtained in Sec. C.4. The craters under the surface of the aluminium samples have an average volume per shot of 28.0 μm^3 at 3.8 J cm^{-2} and 305.2 μm^3 at 25.5 J cm^{-2}, corresponding to an ablated mass of 75.5 and 824.1 pg per pulse, respectively.

In the following, we assumed that all the ablated matter contributes to the plasma emission. Under the RELIBS optimum conditions, which corresponds to an ablation fluence of 3.8 J cm^{-2} and an excitation fluence of 1.1 J cm^{-2}, the absolute LoDs for Mg and Si can be estimated to be about 0.7 fg and 50 fg, respectively. (We checked that there is no noticeable increase of the ablated mass due the presence of the excitation pulse.) On the other hand, the absolute LoDs obtained for LIBS with an ablation fluence of 25.5 J cm^{-2} are 4 fg for Mg and 128 fg for Si. Consequently, the absolute LoDs achieved with RELIBS were improved by a factor of about 5 for Mg and about 3 for Si, when compared with LIBS (with an ablation fluence of 25.5 J cm^{-2}). According to these results, RELIBS appears to be particularly suitable for trace analysis in applications that required caution regarding the amount of mass removed from the sample surface.

D. Conclusion

In this paper, the RELIBS approach was applied for the detection of magnesium and silicon in an aluminium matrix. Our main objectives were to (1) investigate the influence of the experimental parameters (excitation wavelength, interpulse delay, excitation and ablation fluences) on the SNR of the analytical lines, (2) relate whenever possible these results to the general picture of the physical mechanisms involved in RELIBS and (3) evaluate the figures of merits of this technique for analytical purposes.

For our experimental set-up, the optimization of the SNR of the Mg I 285.21 line was achieved for an interpulse delay of 30 ns, an excitation fluence of 1.1 J cm^{-2}, and, an ablation fluence of 3.8 J cm^{-2}. The corresponding time delay of acquisition was 40 ns and the gate width was 3 μs. Moreover, the SNR of the Mg I 285.21 nm exhibits a clear maximum when the excitation wavelength matched the plasma resonant transition of the host Al atoms at 396.15 nm. We have also shown that the ablation fluence is a critical parameter to extract the full potential of the RELIBS technique. Indeed, resonant absorption appeared to be optimum when the ablation fluence was close to the ablation threshold. As the ablation fluence increases, the effect of the on-resonance excitation pulse becomes less and less significant, as a consequence of the higher plasma temperature which decreases the population of the low energy levels. The underlying physical mechanisms have been clarified by comparing the fluorescence signals achieved using RELIBS to those obtained with and without an off resonance excitation pulse. We also investigated the correlation between the damage induced at the surface of the sample and RELIBS performances.

The detection of Mg in an aluminium matrix was chosen here as an illustrative purpose. Nevertheless, the general conclusions presented in this work could likely be also applied, at least qualitatively, to the detection of other elements in other matrices.

In terms of analytical features, the LoDs achieved using RELIBS were comparable to LIBS, but a much lower amount of matter could be ablated from the sample with RELIBS. In fact, the absolute LoDs with RELIBS were improved by a factor of about 5 for Mg and about 3 for Si, in comparison to LIBS (with an ablation fluence of 25.5 J cm^{-2}). For instance, a value of 0.7 fg was achieved for Mg using RELIBS.

This result is consistent with the general conclusion drawn by Cheung and co-workers,[18] that the advantage of RELIBS over LIBS is revealed when a small amount of matter is ablated. Consequently, RELIBS appears to be a great candidate for applications where damage inflicted to the sample must be minimized. For instance, the analysis of artworks (painting, sculpture, *etc.*), artefacts (pottery, coin, *etc.*), jewelleries, forensic samples and microelectronic devices requires cautions regarding the amount of material removed.

Acknowledgements

The authors are grateful to B. Gauthier at the IMI-NRC for assistance in measuring the ablation crater profiles. This work was supported by the Natural Science and Engineering Research Council of Canada (NSERC).

References

1 D. A. Cremers and L. J. Radziemski, *Handbook of laser-Induced breakdown spectroscopy*, John Wiley & Sons, Inc., New York, 2006.
2 A. W. Miziolek, V. Palleschi, and I. Schechter, *Laser-Induced Breakdown Spectroscopy*, Cambridge University Press, New York, 2006.
3 J. P. Singh and S. N. Thakur, *Laser-Induced Breakdown Spectroscopy*, Elsevier, 2007.
4 D. A. Rusak, B. C. Castle, B. W. Smith and J. D. Winefordner, Fundamentals and applications of laser-induced breakdown spectroscopy, *Crit. Rev. Anal. Chem.*, 1997, **27**, 257.
5 J. D. Winefordner, I. B. Gornushkin, T. Correll, E. Gibb, B. W. Smith and N. Omenetto, Comparing several atomic spectrometric methods to the super stars: special emphasis on laser induced breakdown spectrometry, LIBS, a future super star, *J. Anal. At. Spectrom.*, 2004, **19**, 1061.
6 E. H. Evans, J. A. Day, W. J. Price, C. M. M. Smith, K. Sutton and J. F. Tyson, Atomic spectrometry update. Advances in atomic emission, absorption and fluorescence spectrometry and related techniques, *J. Anal. At. Spectrom.*, 2003, **18**, 808.
7 L. St-Onge, M. Sabsabi and P. Cielo, Analysis of solids using laser-induced plasma spectroscopy in double-pulse mode, *Spectrochim. Acta, Part B*, 1998, **53**, 407.
8 V. I. Babushok, F. C. DeLucia Jr., J. L. Gottfried, C. A. Munson and A. W. Miziolek, Double pulse laser ablation and plasma: Laser induced breakdown spectroscopy signal enhancement, *Spectrochim. Acta, Part B*, 2006, **61**, 999.

9 L. St-Onge, V. Detalle and M. Sabsabi, Enhanced laser-induced breakdown spectroscopy using the combination of fourth-harmonic and fundamental Nd:YAG laser pulses, *Spectrochim. Acta, Part B*, 2002, **57**, 121.

10 C. Gautier, P. Fichet, D. Menut, J.-L. Lacour, D. L'Hermite and J. Dubessy, Study of the double-pulse setup with orthogonal beam geometry for laser-induced breakdown spectroscopy, *Spectrochim. Acta, Part B*, 2004, **59**, 975.

11 X. Hou, P. Stchur, K. X. Yang and R. G. Michel, Progress in laser excited atomic fluorescence spectrometry, *Anal. Chem.*, 1998, **17**, 532.

12 H. H. Telle, D. C. S. Beddows, G. W. Morris and O. Samek, Sensitive and selective spectrochemical analysis of metallic samples: the combination of laser-induced breakdown spectroscopy and laser-induced fluorescence spectroscopy, *Spectrochim. Acta, Part B*, 2001, **56**, 947.

13 I. B. Gornushkin, S. A. Baker, B. W. Smith and J. D. Winefordner, Determination of lead in metallic reference materials by laser ablation combined with laser excited atomic fluorescence, *Spectrochim. Acta, Part B*, 1997, **52**, 1653.

14 S. Laville, C. Goueguel, H. Loudyi, F. Vidal, M. Chaker and M. Sabsabi, Laser-induced fluorescence detection of lead atoms in laser-induced plasma: An experimental analytical optimization study, *Spectrochim. Acta, Part B*, 2009, **64**, 347.

15 H. Loudyi, K. Rifai, S. Laville, F. Vidal, M. Chaker and M. Sabsabi, Improving laser-induced breakdown spectroscopy (LIBS) performance for iron and lead determination in aqueous solutions with laser-induced fluorescence (LIF), *J. Anal. At. Spectrom.*, 2009, **24**, 1421.

16 K. Niemax and W. Sdorra, Optical emission spectrometry and laser-induced fluorescence of laser produced sample plumes, *Appl. Opt.*, 1990, **29**, 5000.

17 R. E. Neuhauser, U. Panne, R. Niessner, G. A. Petrucci, P. Cavalli and N. Omenetto, On-line and in situ detection of lead aerosols by plasma-spectroscopy and laser-excited atomic fluorescence spectroscopy, *Spectrochim. Acta, Part B*, 1997, **346**, 37.

18 J. D. Wu and N. H. Cheung, Resonant-enhanced laser-induced breakdown spectroscopy for multielement analysis in laser ablative sampling, *Appl. Spectrosc.*, 2001, **55**, 366.

19 S. L. Lui and N. H. Cheung, Resonance-enhanced laser-induced breakdown spectroscopy: ambient gas effects, *Spectrochim. Acta, Part B*, 2003, **58**, 1613.

20 S. L. Lui and N. H. Cheung, Minimally destructive analysis of aluminium alloys by resonance-enhanced laser-induced breakdown spectroscopy, *Anal. Chem.*, 2005, **77**, 2617.

21 S. L. Lui and N. H. Cheung, Resonance-enhanced laser-induced plasma spectroscopy for sensitive elemental analysis: Elucidation of enhancement mechanisms, *Appl. Phys. Lett.*, 2002, **81**, 5114.

22 S. Y. Chan and N. H. Cheung, Analysis of solids by laser ablation and resonance-enhanced laser-induced breakdown spectroscopy, *Anal. Chem.*, 2000, **72**, 2087.

23 W. L. Yip and N. H. Cheung, Analysis of aluminium alloys by resonance-enhanced laser-induced breakdown spectroscopy: How the beam profile of the ablation laser and the energy of the dye laser affect analytical performance, *Spectrochim. Acta, Part B*, 2009, **64**, 315.

24 D. Cleveland, P. Stchur, X. Hou, K. X. Yang, J. Zhou and R. G. Michel, Resonant laser ablation of metals detected by atomic emission in a microwave plasma and by inductively coupled plasma mass spectroscopy, *Appl. Spectrosc.*, 2005, **59**, 1427.

25 S. T. Dai, J. Jin, W. Lu, R. T. An, L. L. Tai and D. Y. Chen, Resonant laser ablation of copper and its application in microanalysis, *Appl. Phys. A*, 1999, **69**, 167.

26 C. G. Gill, M. Allen, J. E. Anderson, T. N. Taylor, P. B. Kelly and N. S. Nogar, Low-power resonant laser ablation of copper, *Appl. Opt.*, 1996, **35**, 2069.

27 G. Lamouche, M. Dufour, B. Gauthier, V. Bartulovic, M. Hewko and J.-P. Monchalin, Optical delay line using rotating rhombic prisms, Coherence Domain Optical Methods and Optical Coherence Tomography in Biomedicine XI, *Proc. SPIE.*, 2007, **6429**, 64292G.

28 J. M. Liu, Simple technique for measurements of pulsed Gaussian-beam spot sizes, *Opt. Lett.*, 1982, **7**, 196.

29 J. E. Decker, W. Xiong, F. Yergeau and S. L. Chin, Spot-size measurement of an intense CO2 laser beam, *Appl. Opt.*, 1992, **31**, 1912.

30 K. B. S. Eriksson and H. B. S. Isberg, The spectrum of atomic aluminium, Al I, *Ark. Fys.*, 1963, **23**, 527.

31 N. Omenetto, J. Bower, J. Bradshaw, C. A. Van Dijk and J. D. Windefordner, A theoretical and experimental approach to laser saturation broadening in flames, *J. Quant. Spectrosc. Radiat. Transfer*, 1980, **24**, 147.

32 L. M. Cabalin and J. J. Laserna, Experimental determination of laser induced breakdown thresholds of metals under nanosecond Q-switched laser operation, *Spectrochim. Acta, Part B*, 1998, **53**, 723.

